Available online at www.sciencedirect.com
SCIENCE DIRECT®
Journal of Magnetic Resonance 168 (2004) 66–74
JMR Journal of Magnetic Resonance
www.elsevier.com/locate/jmr

Low temperature solid-state NMR experiments of half-integer quadrupolar nuclides: caveats and data analysis

Andrew S. Lipton, Robert W. Heck, Jesse A. Sears, and Paul D. Ellis*

Macromolecular Structure and Dynamics Directorate, WR Wiley Environmental Molecular Sciences Laboratory, Pacific Northwest National Laboratory, Richland, WA 99352, USA

Received 24 October 2003; revised 19 December 2003

Abstract

Solid-state NMR spectroscopy of half-integer quadrupolar nuclides has received a lot of interest recently with the advent of new methodologies and higher magnetic fields. We present here the extension of our previous low temperature method to an 18.8 T system. This new probe entailed a total redesign including a cross coil and variable capacitors that are operational at cryogenic temperatures. The limitations to sensitivity are also discussed; including a new diode network, the utilization of a cryogenic band pass filter, and the consequences of the RF profiles of the coil. Further, details of the spectroscopy of quadrupolar nuclei in a protein are discussed, such as the observation of the outer transitions and how to distinguish them from the desired $\pm 1/2$ transition.

1. Introduction

A long term aim of our research is to obtain a thorough understanding of the bioinorganic chemistry of zinc and magnesium by investigating proteins and synthetic analogues that are designed to mimic both the structure and function of the active sites of metal dependent proteins. One of the vehicles to obtain this objective is through the use of the spectroscopy of zinc and magnesium. The typical oxidation state for zinc and magnesium is +2 and is stable with respect to either oxidation or reduction. With this oxidation state both atoms have a closed shell electron configuration. A direct consequence of this is the absence of characteristic adsorption bands in its UV/Vis spectroscopy. Likewise, EPR spectroscopy is also unavailable.

The basic thrust of our developmental efforts over the past several years has been to characterize Zn^{2+} and Mg^{2+} sites in proteins using NMR spectroscopy. The simplicity of this sentence belies the fact that as little as three years ago most of the NMR community would have described such an experiment as prohibitively difficult. We have developed a means to directly observe these metals in proteins via a low temperature solid-state NMR experiment [1,2]. Therefore, our interest is to exploit this new technology to define the mechanistic details of how divalent metal cations (Zn^{2+}, Mg^{2+}, and Ca^{2+}) augment the chemistry of the proteins to which they bind. Moreover, we want to establish a relationship between magnetic resonance parameters for the metal and the structure of these metals in metalloproteins. The magnetic resonance parameters are sensitive measures of charge, ligand type and number, and the symmetry of the metal site. All of these parameters are a reflection of the potential chemistry that occurs at the metal site. Therefore, such relationships should aid in the development and delineation of the correlation between structure and function for this important class of proteins.

Since our initial report of our low temperature methods, we have refined many of the particulars. These details include the balancing of the double tuned coil used in our 9.4 and 11.7 T probe designs. Likewise, we have developed a cross coil design for our implementation of the low temperature experiment at 18.8 T. We have also explored low temperature duplexers that make more efficient use of the low temperature preamplifier which we introduced in our initial report. Finally, these methods have enabled us to routinely observe Zn^{2+} or

* Corresponding author. Fax: 1-509-376-2303.
E-mail address: paul.ellis@pnl.gov (P.D. Ellis).

1090-7807/$ - see front matter © 2004 Elsevier Inc. All rights reserved.
doi:10.1016/j.jmr.2004.01.008

Mg^{2+} within proteins or protein complexes with molecular weights in excess of 40 kDa. In analyzing the results of these experiments we have noted some special details which are unique to the spectroscopy of these quadrupolar nuclides. Hence, we outline these issues here.

2. Experimental methods

2.1. Probe construction

The design of our current low temperature, double resonance probe implemented at 9.4 T was discussed in a previous paper [1]. The relevant details are that an Oxford continuous flow cryostat is utilized to regulate temperature and transmission lines are used to move the tuning elements out of the magnet (and thus the cold area). The only change we have made to the initial probe circuitry is that the proton channel is now balanced. This design was duplicated with the appropriate change in the internal $\lambda/4$ for use at 11.7 T. While this was easily done, the same cannot be said for extending this technology to 18.8 T. First, we set the constraints that the sample size should be no less than 5 mm and that the low frequency channel of the probe needed to have a 5 or 6 turn solenoid sample coil. The sample size limitation was set to facilitate experiments on the sample at different magnetic fields without unpacking and repacking, as well as to maximize sample within the coil. The number of turns of the solenoid was set to keep the inductance high. This allows for reduced capacitance values in tuning the circuit as well as improving efficiency and RF homogeneity. However, this high inductance prevented the coil from being tunable at 800 MHz. Also, the length of wire used for a 5 turn, 5 mm solenoid is longer than a $\lambda/4$ at 800 MHz. To overcome this situation, we have constructed a cross coil arrangement where the proton coil is a 5 mm saddle coil machined out of oxygen-free copper. This coil is 22 mm long with a 0.019 in. wall thickness and a 12 mm window. A drawing of the cross coil arrangement is depicted in Fig. 1. The proton coil is covered with a Teflon sleeve for insulation from the X-coil, which is a 5 turn solenoid wound from 20 gauge round wire. This geometry (inner saddle coil) was chosen to get the highest proton field possible with minimal power.

Further, the length of transmission line required to go from sample center out of the cryostat (1654 mm) introduced a parasitic resonance into the proton tuning circuitry, which directed most of the power applied away from the sample coil. We have therefore moved our tuning elements back inside the cryostat near the coil arrangement. A schematic diagram of the probe layout is shown in Fig. 2. The variable capacitors for both channels are rated for operation at cryogenic

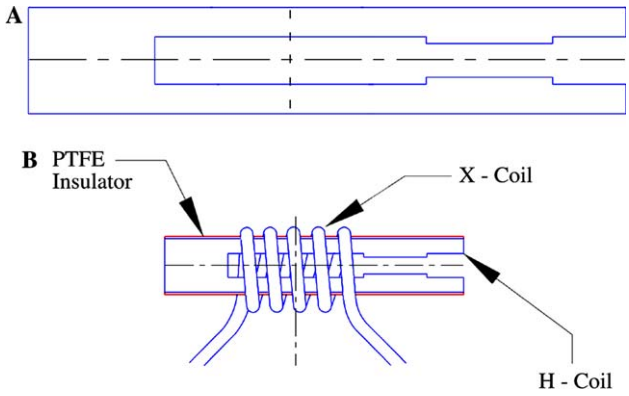

Fig. 1. CAD diagram of the (A) saddle coil machined from O_2-free copper with a length of 22 mm, wall thickness of 0.019 in., and a 12 mm window and (B) the cross coil arrangement showing the Telfon sleeve wrapping the inner coil and the outer five turn saddle coil.

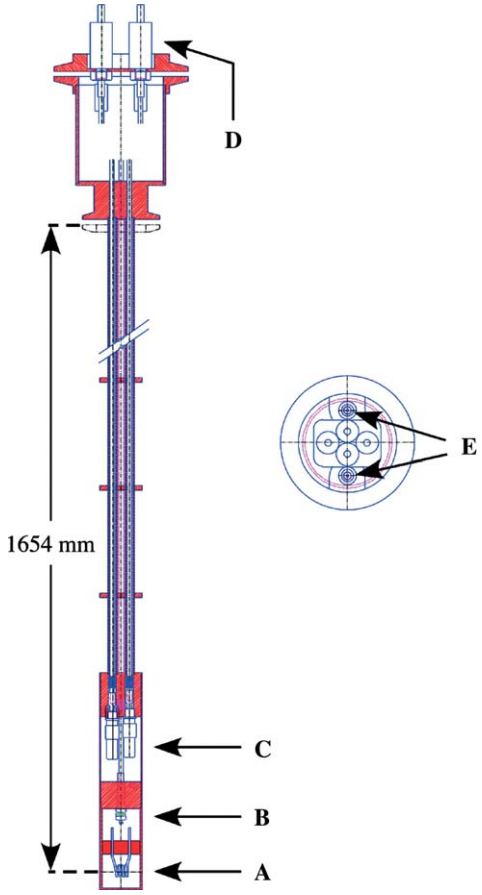

Fig. 2. CAD drawing of the cryogenic probe developed for use in an Oxford cryostat with a length of 1654 mm and an opening of 30 mm, where (A) is the cross coil at sample center, (B) the location of the proton channel capacitors, Voltronics NMKT10HVK (1–10 pF) for tune and NMAT25HVK (1–23 pF) for match, (C) the observe tune and match capacitors which are both special order Voltronics V2642 (3–23 pF) cryogenic, variable capacitors, (D) four vacuum tight, motion feed-thru's with o-ring seals (which were manufactured in-house), and (E) RF feed-thru's for supplying power to the probe head. Mechanical and RF couplings have been omitted for clarity.

temperatures, and the adjustments are made with vacuum tight rotary feed-thru's (indicated on Fig. 2) [3]. This probe functions well at 18.8 T giving a 5.5 μs proton $\pi/2$ pulse width with only 20 W. The Hartmann-Hahn condition [4] for ^{67}Zn only requires 30 W to match that proton field and 110 W gives a 5.5 μs ^{67}Zn selective $\pi/2$.

2.2. Transmitter/receiver network

The network at 9.4 T now consists of an active Transmitter/Receiver (T/R) switch in which the through diodes are back-to-back PIN diodes (for increased isolation) from the high power amplifier to a N-type tee and then into a 27 MHz band pass filter (Microwave Circuits) with a 10 MHz pass band designed to operate while immersed in liquid N_2 and then to the NMR probe. The PIN diodes are synchronized to the receiver gate generated by the console. The other side of the tee is a $\lambda/4$ at 25 MHz, which goes to the cryogenic Miteq preamplifier (input protected by eight sets of anti-parallel 1N914 diodes to ground, four sets on each end of a diode to ground box).

The consoles used in these experiments are as follows: Varian Infinity at 9.4 T, Varian Unity at 11.7 T, and Varian Inova at 18.8 T. For all instruments the broadband preamp supplied with the console was not utilized. Rather a cryogenic narrow band tuned (5 MHz centered on the ^{67}Zn frequency) preamp from Miteq was used (immersed in $N_2(l)$—77 K) at each field. The network described above was put into use on the 9.4 T system. The other systems use passive networks with 1N914 diodes and standard high power low pass RF filters. The outputs of the cryogenic preamplifiers are routed back into the standard console downconverter, then into the receiver boards. On the 11.7 and 18.8 T systems, we diverge from the standard configuration again as the output from the narrow band receiver is routed to the wideline ADCs (5 MHz). This allows use of the narrow band audio filters (typical value is ±50 kHz) for further noise reduction.

2.3. Simulations

The simulations were all performed using the program SIMPSON [5] on several systems (SGI Origin 2000—8 CPUs and 23-Racksaver Dual P4 2.4 GHz Xeon nodes combined with 8-Racksaver Dual Pentium III 1.26 GHz nodes into a Beowulf cluster running the Rocks clustering software utilizing a gigabit Ethernet interconnect).

3. Results and discussion

There are some caveats for using these transmission line probes, which we will now discuss. The first pertains to the lines themselves, we have found that these lines must be airtight. That applies not simply to the top (room temperature) end, but to the bottom (which resides inside the cryostat) as well. Sealing the top is a necessity, as even a small pinhole will cause the lines to fill with condensed liquid N_2. An indication of this is that within 4 h (depending upon the size of the leak) the proton tuning will begin to drift rapidly. This can push the tuning as much as 10 MHz lower than the proton frequency. Caution should be taken in warming this probe, as the transmission line is now a pressurized vessel. The cold end must also be sealed tightly as a partial pressure of helium in the transmission lines will cause that line to break down and arc. We have also discovered a frequency dependence to the materials used in plugging the lines. Our initial plugs were machined out of Teflon, however, this material when cold will arc at 500 MHz and above. We have switched to using Vespel and have had no difficulties with it at any of our fields. To make the upper seal air tight we use a non-conductive epoxy, and a fine coating of epoxy between the lower plugs and the stainless steel makes the other seal. The Teflon plugs also had the habit of leaking after several thermal cycles, and over time (4–6 months) the probe would condense enough water inside the transmission lines that they would have to be opened, dried, and resealed.

The other issue with these probes is a question of optimal sensitivity. The whole purpose of our method is to push sensitivity as high as achievable to observe these spins in a dilute environment. The target of our interest is to obtain NMR data from a nuclide with a mass of 25 or 67 Da in a protein of typically 30–50 kDa. We have found that the stainless steel construction of our transmission line is still necessary to prevent undue heat being conducted down to the sample area. However, this introduces a time lag to the probe reaching thermal equilibrium. An indication of the thermal equilibration is that the proton tuning will drift slightly over the first 12 h after being cooled from room temperature.

Once the probe has reached thermal equilibrium, the noise floor is then at its minimum value while the signal content should be at its maximum. The ambient noise of the system is the next target when boosting sensitivity. The cryogenic preamp has already demonstrated a reduction in noise as the typical room temperature preamplifier has a noise figure of approximately 1.3 versus nominally 0.2 for one at 77 K. We have pursued other possible noise sources such as the low pass filter between the probe and the receiver network. As detailed above, we have incorporated a hermetically sealed band pass filter capable of being submerged in liquid N_2 into our system. The surprising information was that this filter did not improve its noise figure upon cooling to 77 K. However, the overall effect of the new PIN diodes combined with the new filter was an improvement in S/N of around 15%.

Generally, when investigating half-integer quadrupolar nuclides by solid-state NMR methods the principal observable is the central or $\pm 1/2$ transition for that spin. The experiment we are utilizing is CP [6] followed by a CPMG train of π pulses [7]. Consider a spin 5/2 nucleus such as ^{67}Zn or ^{25}Mg with an unknown value of C_q; there are two possible extremes that one can find with these experiments; first, for a small value of C_q where the central transition lineshape is narrow and totally contained within the excitation region, and second that C_q is large and expected lineshape is quite broad (requiring several subspectra to reconstruct the complete spectrum [8]). A further question is the selectivity of these experiments for the $\pm 1/2$ transition. These transitions ($|3/2| \Longleftrightarrow |1/2|$; $|5/2| \Longleftrightarrow |3/2|$) all overlap as indicated in the simulated data in Fig. 3 where the top spectrum is a spin 5/2 lineshape with an η of 1 and the lower spectrum is the same except with an η of 0. One can see that for $\eta = 1$ there is significant overlap of intensity centered on the $\pm 1/2$ transition.

With a small value of C_q one has to consider the strength of the RF fields used during the echo train. Too strong a pulse will severely distort the resulting data [9] set such that it does not resemble a pure quadrupole lineshape (and may prevent a simulation optimization from converging). The regimes to avoid are where the RF field strength (ω_{RF}) for the π pulses is comparable to the quadrupolar splitting, i.e.,

$$|\omega_Q/\omega_{RF}| > 3 \tag{1}$$

and where the ω_{RF} is less than the second order quadrupolar lineshape, i.e.,

$$2\omega_Q^2/(\omega_0\omega_{RF}) > 0.1. \tag{2}$$

Here, ω_Q is defined as

$$\omega_Q = C_q/2I(2I-1) \tag{3}$$

or $C_q/20$ for a $I = 5/2$. This is exemplified in the ^{25}Mg spectra of Fig. 4. The top two spectra are magnesium acetate acquired with CP and a π pulse of 4 μs and an optimized simulation with quadrupole parameters of $C_q = 3.02$ and $\eta_q = 0.72$. The bottom spectra are the same sample acquired utilizing a 15 μs π pulse width and its respective simulation calculated with $C_q = 2.81$ MHz with $\eta_q = 0.68$. These parameters were independently optimized showing that by using an exact density matrix calculation one can approximate the lineshape to extract values of C_q and η to within 10% error. However these numbers would be less reliable for those nuclides that have significant shift anisotropy contributions to the lineshape, such as $^{63/65}$Cu or $^{87/89}$Rb [10,11], as well as distortions due to pulse width. It is also worth noting that there are values of C_q where one cannot fulfill the inequalities mentioned above. For example, a ^{25}Mg or ^{67}Zn ($\omega_0 \approx 25$ MHz at 9.4 T) with a C_q larger than 8 MHz does not satisfy the requirements, hence one would have to rely on using an exact calculation or use multiple overlapping experiments to piece the lineshape together.

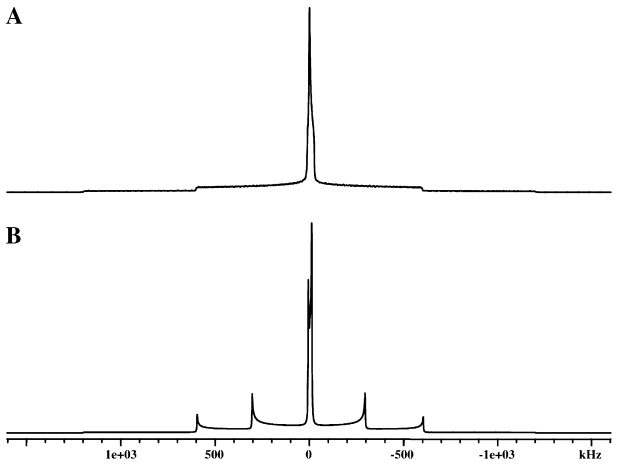

Fig. 3. Simulated lineshapes for a spin 5/2 nucleus at 9.4 T with a C_q of 4 MHz an η of (A) 1.0 and (B) 0.0.

In the second extreme, where C_q is large, the problem is more difficult to quantify. The ^{67}Zn solid-state NMR spectra of each of the protein samples investigated thus far seems to have a value of η_q near 1. Under the conditions of our experiment, it has been difficult to determine the edges of our lineshapes as each side trails off slowly to baseline rather than a distinct break. However, using the width of the center feature one can estimate the value of C_q. The question of selectivity further complicates these determinations as the outer transitions are also excited (even with selective pulses). The $3/2 \Longleftrightarrow 1/2$ transition has a Hartmann-Hahn match condition very close to the $\pm 1/2$ transition [12].

$$\gamma_H B_{1H} = \alpha\gamma_{Zn} B_{1Zn}, \tag{4}$$

$$\alpha = [I(I+1) - m(m-1)]^{1/2}, \tag{5}$$

where γ and B_1 are the gyromagnetic ratio and RF field for each respective nucleus. The factor α for a 5/2 spin (like ^{67}Zn or ^{25}Mg) is 3 for the $\pm 1/2$ transition, however for the $3/2 \Longleftrightarrow 1/2$ transition this factor is $\sqrt{8}$. The theory behind the single and multiple quantum CP match conditions has been discussed previously [13]. The problem is further complicated when one considers the RF is most likely not homogeneous across the whole sample. This is worse still if the RF profile is different for each channel (hot spots on different turns of the coil). The RF profile can (and should) be checked using a network analyzer to probe the tuning deflections on each channel as a function of moving a conductive wafer inside the coil. Examples of this are shown in Fig. 5 where we have mapped a double tuned solenoid probe used at 11.7 T and the cross coil 18.8 T probe. One should note the apparent "hot spot" on the saddle coil, this region of the coil is the loop (or turn) away from the leads. One should expect a gain in S/N of 20–30% if the two profiles can be flattened out. The double tuned

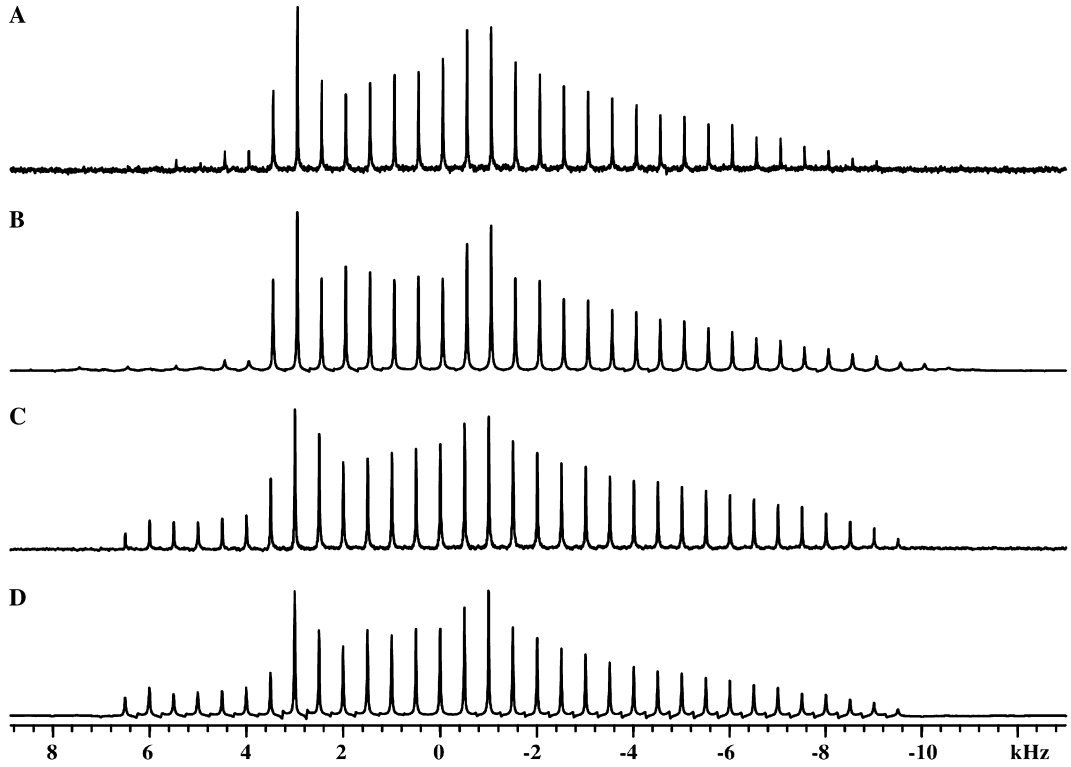

Fig. 4. Experimental and simulated ^{25}Mg NMR data at 9.4 T and 50 K. The experimental spectrum of $Mg(OAc)_2 \cdot 4H_2O$ acquired using 4 μs π pulses is shown in (A) with the simulation using finite pulse widths in (B) and the experimental spectrum acquired using 15 μs π pulses and its corresponding simulation are in (C) and (D), respectively.

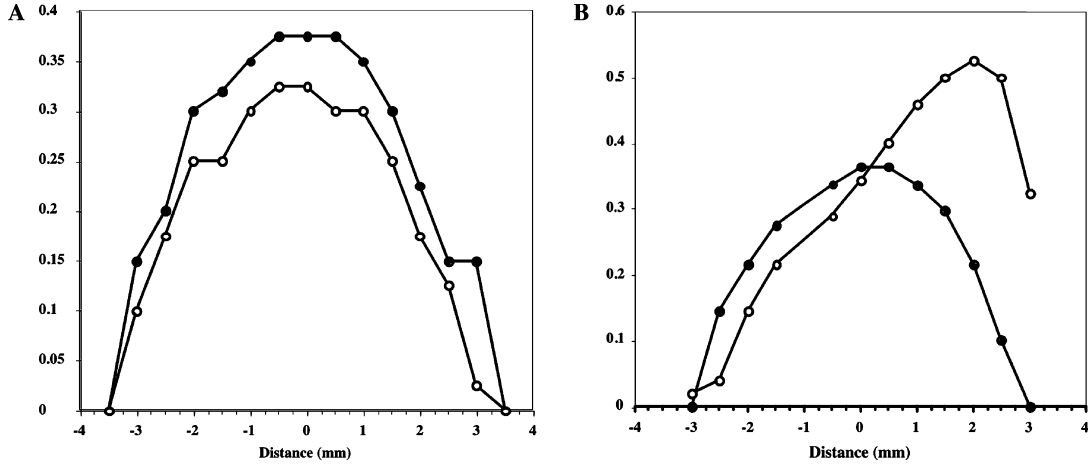

Fig. 5. RF field plots for the proton and X-channels of (A) double tuned solenoid and (B) cross coil where the *x*-axis is the position of the conductive disk from the center of the coil. The open circles (-○-) are the proton channel and the filled circles (-●-) are the X circuit.

solenoid suffered in this way, however with a balanced proton channel, the RF profile was centered to match the low frequency side (which is not balanced in this case). This in effect improves the RF homogeneity across the coil and allows more of the sample to be at the Hartmann-Hahn match condition which results in an increase in S/N. This issue has been recognized by commercial probe vendors and they have directed their efforts toward improving their technology [14].

The data in Fig. 6 shows a ^{67}Zn spectrum of human carbonic anhydrase (CA) II at pH 5 collected at 9.4 T (sample mass 125 mg, and ≈15% water), which is a perfect example of the problem. When this work was started the expected width of the lineshape was unknown, except that we anticipated a large value of C_q. The ab initio molecular orbital theory predicted C_q was on the order of 35–40 MHz, which would have an edge of the lineshape around 1–1.3 MHz higher in frequency

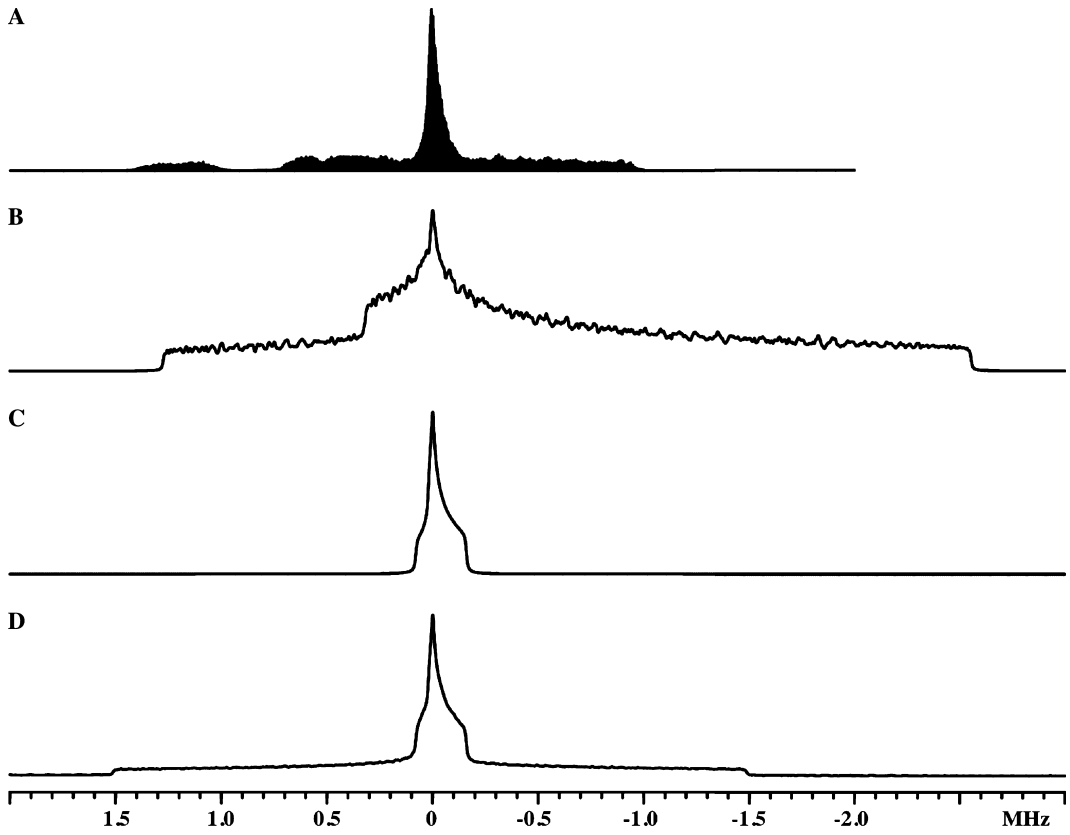

Fig. 6. Experimental and simulated ^{67}Zn NMR data for human carbonic anhydrase (pH 5), where (A) is the experimental data set acquired at 10 K and 9.4 T and (B) and (C) are simulations using ideal pulses and C_qs of 40 and 10 MHz, respectively. The spectrum in (D) is calculated using the parameters of (C) including the contributions from the $3/2 \Longleftrightarrow 1/2$ and $5/2 \Longleftrightarrow 3/2$ transitions.

than our isotropic chemical shift. To acquire this data the sample was cooled to 10 K and the CP/QCPMG experiment was applied stepping the transmitter frequency 30 kHz from −900 to +660 kHz, then finally from +1.19 to +1.33 MHz in an attempt to define the edge of the spectrum. Each experiment represents two contacts of CP and 512 transients taken every 30 s (or ≈4.3 h). As it turns out the narrow species in the center was the whole ±1/2 spectrum (rather than an impurity with a narrow lineshape) [15]. The shelf of spikes in both directions was indeed the $3/2 \Longleftrightarrow 1/2$ transition, as verified by data collection at other fields. The simulated powder spectrum in Fig. 6B is the ±1/2 transition alone for a C_q of 40 MHz, while the simulation in Fig. 6C was calculated using a value of 10 MHz. The spectrum in Fig. 6D represents a simulation combining all of the transitions for a C_q of 10 MHz. These predicted data sets were calculated using ideal pulses.

In an attempt to analyze this data a SIMPSON calculation was written utilizing finite pulse widths and a complete density matrix calculation. The results of that calculation demonstrated that the QCPMG train also populates the outer transitions even with selective π pulses. To simulate more closely how the experiment is actually performed the transmitter frequency in the simulation was moved every 20 kHz (from −200 to +200 kHz, and in coarser steps outside that range), a dataset "acquired" using a QCPMG sequence (no CP), followed by a sky projection of the data to reconstruct it. The resulting simulation assuming a 10 MHz C_q is compared with the experimental spectrum in Fig. 7.

The simplest method to determine if the completed data set falls into this situation (assuming you know something about the sample purity) is to simulate the lineshape using only the central transition as in Fig. 6B and compare the width of the central portion of the lineshapes to see if the calculated spectrum adequately describes the breadth of this feature. If not (as in this case) the likelihood is that the outer transitions are also being observed. The spectrum can also be acquired at higher field (i.e., from 9.4 to 18.8 T), which allows the separation of the second order quadrupolar lineshape from the first order lineshape of the outer transitions. By doubling the field the central transition lineshape has half of the width of the lower field, while the $3/2 \Longleftrightarrow 1/2$ contribution remains the same (thus dropping in intensity relative to the central transition). The results of this are shown in Fig. 7C where we have the simulated 9.4 T data, and then replicate the calculation changing only the field to 18.8 T. One could

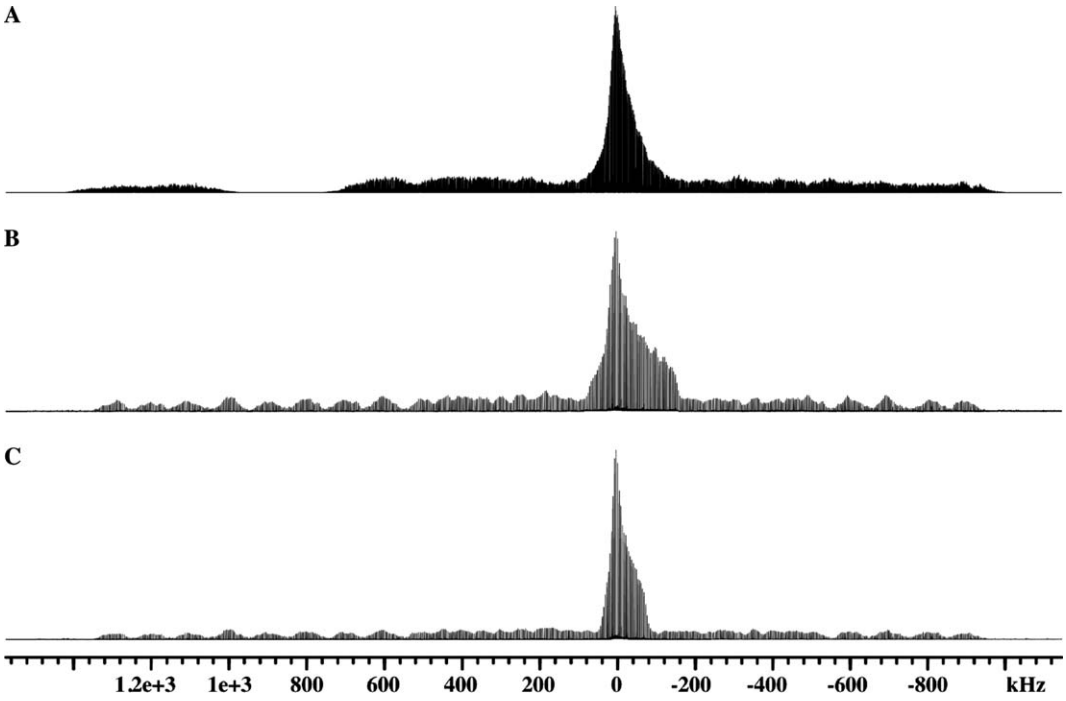

Fig. 7. (A) Experimental ^{67}Zn spectrum of CA, pH 5, from Fig. 6A and simulated QCPMG experiment for a C_q of 10 MHz and an η of 1.0 at (B) 9.4 T and (C) 18.8 T allowing all observable coherences to be detected. The offset was stepped from −200 to 200 kHz in 20 kHz increments, then in 50 kHz steps from 200 to 500 and −200 to −500 kHz, finally in 100 kHz steps out to −800 and +1300 kHz. Each spectrum is the result of a sky projection.

therefore use this method to completely map out the outer transitions as well, if sufficient sensitivity is available (and spectrometer time).

The data shown in Fig. 8 represents the culmination of the efforts discussed in this paper. We can now acquire low temperature data at 18.8 T to verify our low field results. Shown is a sky projection of ^{67}Zn CP/QCPMG experiments on 60 mg (≈10–15% water) of hCA at pH 5. One can fit these data using a C_q of 9.6 MHz (shown in the figure as a powder lineshape). Each individual spectral component utilized in the sky projection of Fig. 8 was acquired at 10 K in 45 min of experiment time (128 transients with a 20 s repetition rate). The lineshape for hCA at pH 5 acquired at 18.8 T trails off on each edge, however with more signal to noise the rest of the outer transitions can be detected. Each section of the spectrum at 18.8 T was acquired about six times faster than the corresponding spectrum at 9.4 T. This gain was achieved even with the sample size reduced by a factor of two and a lower filling factor with the change in coil geometry.

One could also envision the case where there are two legitimate overlapping lineshapes of both a large and small C_q. Under these circumstances the outer transitions for the small C_q species could potentially mask the lineshape of the broad species. The solution is the same as above; repeat the experiment at higher field paying close attention the relative ratios of each respective component. A doubling of the magnetic field strength will narrow each second order lineshape leaving the first order lineshape of the outer transitions

Another feature to the calculated data of Fig. 7 is that there still seems to be distinct discontinuities where the central transition portion of the lineshape ends. This is not the case in our experimental data. Indeed, even in those cases where the outer transitions have not been observed, the lineshapes are not ideal. This is partially attributable to static disorder about the metal, which has been observed before in lyophilized powders via EXAFS [16]. However, our data are not significantly improved when utilizing a frozen solution (10% glycerol) while the EXAFS data were. We have not attempted to acquire one of these data sets via direct observation (no CP). However, with the proper doping of paramagnetics to lower the metal's T_1 (we typically do not determine this value) and a low molecular weight system (<5 kDa), one should have sufficient sensitivity to address the question of whether the CP is responsible for this distortion. Most likely is that with C_q's on this order these non-crystalline samples have even more disorder introduced by cooling the sample to these temperatures resulting in these features being washed out. That in combination with the QCPMG train populating multiple states gives rise to the lineshapes we observe.

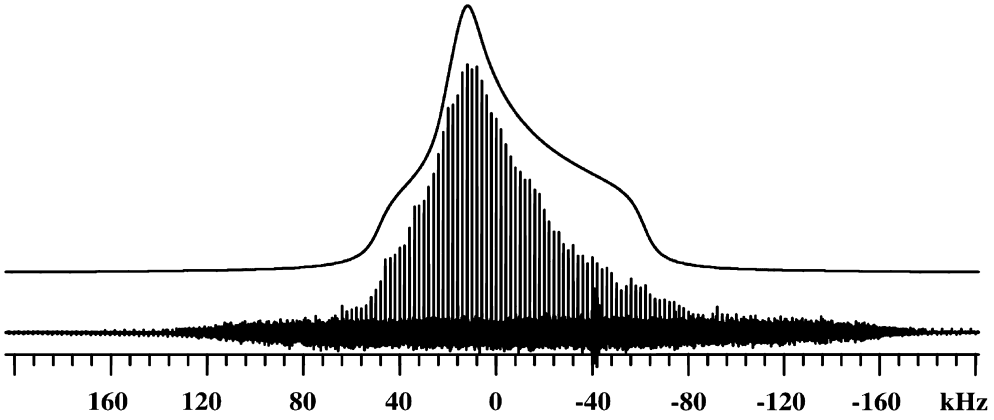

Fig. 8. Experimental ^{67}Zn spectrum of CA, pH 5, acquired at 18.8 T and 10 K and a simulated powder spectrum of a central transition lineshape corresponding to a C_q of 9.6 MHz. The experimental spectrum is the result of a sky projection of individual datasets moving the spectrometer frequency in 10 kHz steps.

4. Conclusions

We have successfully adapted our low temperature solid-state NMR methodology from a 9.4 T system to a 11.7 T cryostat (both widebore magnets, 49 mm opening in the Oxford cryostat). Analysis of data acquired on ^{67}Zn-labeled proteins has necessitated a move to higher fields to facilitate distinguishing the central from the outer transitions. We have therefore extended this technology further by constructing a probe at 18.8 T, within the space requirements of the medium bore (30 mm opening in the Oxford cryostat). This new probe makes use of new components that can function under cryogenic temperatures as well as a cross coil, making the tuning more straightforward. This new design lends itself easily to the idea of adding a third channel by double tuning of the solenoid coil. A prototype of this probe is being constructed for use on our 11.7 T system. This probe will also serve to remove any high temperature noise from the variable capacitors as well as improve the efficiency by removing the need for long transmission lines.

We have tested an active network and a cryogenic RF filter to further reduce our noise floor. The cryogenic aspect of the filter appears unnecessary, however use of a band pass is preferable to a low pass filter. The combination has resulted in a gain of 15% of our S/N. The next target for noise reduction will be moving the probe tuning into the cryogenic area of the probe.

We have also demonstrated the RF field strength dependence on a determination of C_q. While it is not realistic to expect undistorted lineshapes for our non-crystalline protein samples, this especially applies to large C_q lineshapes requiring multiple experiments with shifting offsets where the quadrupole parameters can still be extracted. We have excellent sensitivity and while we can now inconveniently observe the outer transition lineshapes, we can differentiate them from the desired central transition. The addition of higher fields helps us to make this determination as well as boosting sensitivity higher. These methods have afforded us the opportunity to examine spins in rare environments, providing a novel and complementary information to X-ray crystallographic methods.

Acknowledgments

This work was supported in part by the National Institutes of Health (Federal Grant EB002050) and by the Department of Energy Office of Biological and Environmental Research Program under Grants KP11-01-01: 24931 and 41055. The research was performed in the Environmental Molecular Sciences Laboratory (a national scientific user facility sponsored by the DOE Biological and Environmental Research) located at Pacific Northwest National Laboratory and operated for DOE by Battelle. We also thank Yvonne Rodriguez for help in generating the human carbonic anhydrase sample.

References

[1] A.S. Lipton, J.A. Sears, P.D. Ellis, A general strategy for the NMR observation of half-integer quadrupolar nuclei in dilute environments, J. Magn. Reson. 151 (2001) 48–59.
[2] A.S. Lipton, G.W. Buchko, J.A. Sears, M.A. Kennedy, P.D. Ellis, ^{67}Zn solid-state NMR spectroscopy of the minimal DNA binding domain of human nucleotide excision repair protein XPA, J. Am. Chem. Soc. 123 (2001) 992–993.
[3] Note that some commercially available rotary feed-thru's have magnetic components and will not hold vacuum after being inside a magnetic field.
[4] S.R. Hartmann, E.L. Hahn, Nuclear double resonance in the rotating frame, Phys. Rev. 128 (1962) 2042.
[5] M. Bak, J.T. Rasmussen, N.C. Nielsen, SIMPSON: a general simulation program for solid-state NMR spectroscopy, J. Magn. Reson. 147 (2000) 296.

[6] A. Pines, M.G. Gibby, J.S. Waugh, Proton enhanced nuclear induction spectroscopy. A method for high resolution NMR of dilute spins in the solids, J. Chem. Phys. 56 (1972) 1776.
[7] (a) H.Y. Carr, E.M. Purcell, Phys. Rev. 94 (1954) 630;
(b) S. Meiboom, D. Gill, Rev. Sci. Instrum. 29 (1958) 688.
[8] (a) A.S. Lipton, T.A. Wright, M.K. Bowman, D.L. Reger, P.D. Ellis, Solid-state ^{67}Zn NMR spectroscopy in bioinorganic chemistry. Spectra of 4- and 6-coordinate zinc pyrazolylborate complexes obtained by management of proton relaxation rates with a paramagnetic dopant, J. Am. Chem. Soc. 124 (2002) 5850–5860;
(b) A. Medek, L. Frydman, l. Frydman, Central transition nuclear magnetic resonance in the presences of large couplings: cobalt-59 nuclear magnetic resonance of cobaltophthalocyanines, J. Phys. Chem. 103 (1999) 4830–4835.
[9] F.H. Larsen, H.J. Jakobsen, P.D. Ellis, N.C. Nielsen, High-field QCPMG-MAS NMR of half-integer quadrupolar nuclei with large quadrupole couplings, Mol. Phys. 95 (1998) 1185–1195.
[10] (a) S. Kroeker, R.E. Wasylishen, A multinuclear magnetic resonance study of crystalline tripotassium tetracyano-cuprate, Can. J. Chem. 77 (1999) 1962–1972;
(b) P.R. Bodart, J.-P. Amoureux, Y. Dumazy, R. Lefort, Theoretical and experimental study of quadrupolar echoes for half-integer spins in static solid-state NMR, Mol. Phys. 98 (2000) 1545–1551;
(c) A.S. Lipton, J.V. Hanna, in preparation.
[11] (a) J.T. Cheng, J.C. Edwards, P.D. Ellis, Measurement of quadrupolar coupling constants, shielding tensor elements and the relative orientation of quadrupolar and shielding tensor principal axis system for Rb-87 and Rb-85 nuclei in rubidium salts by solid-state NMR, J. Phys. Chem. 94 (1990) 553–561;
(b) J.M. Koons, E. Hughes, H.M. Cho, P.D. Ellis, Extracting multitensor solid-state NMR parameters from lineshapes, J. Magn. Reson. A. 114 (1995) 12–23;
(c) T. Vosegaard, J. Skibsted, H. Bildsøe, H.J. Jakobsen, Quadrupole coupling and anisotropic shielding from single-crystal NMR of the central transition for quadrupolar nuclei. ^{87}Rb NMR of $RbClO_4$ and Rb_2SO_4, J. Magn. Reson. A. 122 (1996) 111–119.
[12] (a) S. Vega, Phys. Rev. 23 (1981) 3152;
(b) T.H. Walter, G.L. Turner, E. Oldfield, Oxygen-17 cross-polarization NMR spectroscopy of inorganic solids, J. Magn. Reson. 76 (1988) 106;
(c) R.K. Harris, G.J. Nesbitt, Cross Polarization for quadrupolar nuclei-proton to sodium-23, J. Magn. Reson. 78 (1988) 245–256;
(d) A. Vega, CP/MAS of quadrupolar $S = 3/2$ nuclei, Solid State NMR 1 (1992) 17.
[13] (a) S.E. Ashbrook, S. Wimperis, Single- and multiple-quantum cross polarization in NMR of quadrupolar nuclei in static samples, Mol. Phys. 98 (2000) 1–26;
(b) J.-P. Amoureux, M. Pruski, Theoretical and experimental assessment of single- and multiple-quantum cross-polarization in solid state NMR, Mol. Phys. 100 (2002) 1595–1613.
[14] J.A. Stringer, C.E. Bronnimann, Advances in RF field overlap and homogeneity in triple resonant CPMAS probes, in: Oral Presentation at the 43rd Experimental Nuclear Magnetic Resonance Conference, April 14–19, 2002.
[15] A.S. Lipton, R.W. Heck, P.D. Ellis, Zinc solid-state NMR spectroscopy of human carbonic anhydrase. Implications for the enzymatic mechanism, J. Am. Chem. Soc., in press.
[16] G.W. Buchko, N.J. Hess, M.A. Kennedy, Carcinogenesis 21 (2000) 1051–1057.